Near-field: A finite-difference time-dependent method for simulation of electrodynamics on small scales

Arunima Coomar, Christopher Arntsen, Kenneth A. Lopata, Shlomi Pistinner, and Daniel Neuhauser[a)]
Department of Chemistry and Biochemistry, UCLA, Los Angeles, California 90095-1569, USA

(Received 6 April 2011; accepted 1 August 2011; published online 29 August 2011)

We develop near-field (NF), a very efficient finite-difference time-dependent (FDTD) approach for simulating electromagnetic systems in the near-field regime. NF is essentially a time-dependent version of the quasistatic frequency-dependent Poisson algorithm. We assume that the electric field is longitudinal, and hence propagates only a set of time-dependent polarizations and currents. For near-field scales, the time step (dt) is much larger than in the usual Maxwell FDTD approach, as it is not related to the velocity of light; rather, it is determined by the rate of damping and plasma oscillations in the material, so $dt = 2.5$ a.u. was well converged in our simulations. The propagation in time is done via a leapfrog algorithm much like Yee's method, and only a single spatial convolution is needed per time step. In conjunction, we also develop a new and very accurate 8 and 9 Drude-oscillators fit to the permittivity of gold and silver, desired here because we use a large time step. We show that NF agrees with Mie-theory in the limit of small spheres and that it also accurately describes the evolution of the spectral shape as a function of the separation between two gold or silver spheres. The NF algorithm is especially efficient for systems with small scale dynamics and makes it very simple to introduce additional effects such as embedding. © *2011 American Institute of Physics*. [doi:10.1063/1.3626549]

I. INTRODUCTION

The finite-difference time-dependent method (FDTD, also labeled here as Maxwell's FDTD) is one of the main methods for quantitative simulations of electromagnetic systems[1–5] (alternatives include, e.g., the discrete dipole approximation (DDA),[6–8] plasmon hybridization,[9] and frequency-domain approaches[10,11]). Recently, there have been much efforts directed at merging Maxwell's FDTD with the time-dependent Schrödinger (or alternatively Heisenberg or Bloch) equations for describing near-field dynamics and the effects on or of molecules (see e.g.,[12]). A difficulty in these simulations, however, is the tiny time step required in FDTD. Here, we show how to circumvent the time step difficulty for small structures (below 50 nm).

In Maxwell's FDTD, the time step dt needs to be smaller than $dx/(\sqrt{3}c)$, where dx is the minimal grid spacing and c is the velocity of light, ~137 a.u. For example, for near field (NF) structures where the features are as small as 0.1 nm, $dt \sim 0.008$ a.u $= 0.2$ attoseconds. This is a tiny step when considering that in real-time electronic dynamics dt can be as big as ~1 a.u.

A simple solution is to realize that in the near-field world, where the structures are much smaller than the wavelength, the electric field is mostly unrelated to the velocity of light; instead, the dominant component of the electric field is longitudinal, i.e., the quasistatic gradient of the Coulomb integral over the instantaneous charge distribution:

$$\mathbf{E}_{\text{near field}}(\mathbf{r}, t) = -\frac{\nabla}{4\pi\varepsilon_0}\int \frac{\rho(\mathbf{r}', t)}{|\mathbf{r} - \mathbf{r}'|} d^3\mathbf{r}'. \quad (1)$$

We therefore propose here to propagate only the time-dependent density and currents (see precise definitions later), and to assume that the electric field is longitudinal. The relation between electric fields and currents remains, however, exactly as in Maxwell's FDTD so that the crucial frequency dependence of the permittivity, $\varepsilon(\mathbf{r}, \omega)$, is fully captured. The overall approach is therefore labeled NF. NF is simply the time dependent version of the usual frequency dependent Poisson approach (see, e.g., Ref. 11).

For the evolution of NF in time, we develop here a leapfrog approach, analogous to Yee's method for Maxwell's FDTD. As we show, a very large time step is feasible in NF (2.5 a.u., ~300 times bigger than the minimum time step in FDTD for small features) at a price of a convolution (Coulomb integral) each time step.

Note that as a matter of semantics we use the term NF rather than quasistatic. The latter term could be misleading as the frequencies involved here are as high as in any FDTD simulations (up to 6 eV in our simulations); the NF label only implies that the length scales are much smaller than the wavelength of the light. Also, formally NF is also a finite-difference time-dependent method, but for brevity we often label it just as NF.

Finally, we develop here a new and very accurate, 8- and 9-oscillator fit (containing a total of 24-27 terms) to the permittivity of gold and silver. The fit yields very closely the experimental values between near IR and UV. The main feature

a)Author to whom correspondence should be addressed. Electronic mail: dxn@chem.ucla.edu.

in the new fit is that all damping constants (explained below) are not overly large, so the fit can be used with the large time steps allowed in NF.

The remainder of the paper is developed as follows. The method is explained in detail in Sec. II, the fit is examined in Sec. III, and Sec. IV shows absorption profiles for both single spheres and dimers; the results are favorably compared to Mie theory (for single spheres) and numerical Maxwell's FDTD simulations (metal dimers). Discussion and conclusions follow in Sec. V.

II. METHODOLOGY

A. Overall equations

For each material the permittivity is represented as a sum of Drude oscillators:

$$\varepsilon(\omega) = \varepsilon_\infty + \varepsilon_0 \sum_{j=1}^{N_j} \frac{\beta_j}{\bar{\omega}_j^2 - i\alpha_j\omega - \omega^2}, \tag{2}$$

where $\alpha_j, \bar{\omega}_j, \beta_j$,are (real) material-dependent parameters; most studies use $N_j \sim$ 2–4 Lorentzians (i.e., Drude-oscillators) (see e.g., Ref. 13 and references therein), but as mentioned, here we apply 8-9 Lorentzians to give an excellent fit over a wide frequency range. Further, the first version developed here requires a spatially constant ε_∞ (here we use $\varepsilon_\infty = \varepsilon_0$); the next version will relax this requirement, as explained in the conclusions. Equation (2) is natural for metals, so in this first paper we only simulate metals + vacuum.

We aim for an overall time-dependent density which fulfills the continuity equation,

$$\frac{\partial\rho}{\partial t} = -\nabla\cdot\mathbf{J}, \tag{3}$$

such that the permittivity will be associated with an overall polarization which fulfills the Poisson equation

$$\nabla\cdot(\varepsilon(\mathbf{r},\omega)\tilde{\mathbf{E}}(\mathbf{r},\omega)) = 0, \tag{4}$$

where the Poisson equation vanishes since the density is due to the polarization in the metal, and there are no free charges in this version (they could be straightforwardly added). Also, $\tilde{\mathbf{E}}$ refers to the field in frequency space. The frequency-dependent Poisson equation and the continuity equation are both fulfilled if we define currents and polarizations $\mathbf{J}_j(\mathbf{r},t)$, $\mathbf{P}_j(\mathbf{r},t)$, which are evolved as follows:

$$\frac{\partial\mathbf{P}_j(\mathbf{r},t)}{\partial t} = \mathbf{J}_j(\mathbf{r},t), \tag{5}$$

$$\frac{\partial\mathbf{J}_j(\mathbf{r},t)}{\partial t} = -\alpha_j(\mathbf{r})\mathbf{J}_j(\mathbf{r},t) - \bar{\omega}^2(\mathbf{r})\mathbf{P}_j(\mathbf{r},t) + \varepsilon_0\beta_j(\mathbf{r})\mathbf{E}(\mathbf{r},t), \tag{6}$$

such that the total current and polarization are

$$\begin{aligned}\mathbf{J}(\mathbf{r},t) &= \sum_j \mathbf{J}_j(\mathbf{r},t),\\ \mathbf{P}(\mathbf{r},t) &= \sum_j \mathbf{P}_j(\mathbf{r},t).\end{aligned} \tag{7}$$

Equations (5)–(7) give the usual relation between the current and the electric field, i.e., when transforming from time to frequency, then at each point in space

$$\begin{aligned}\tilde{\mathbf{J}}(\mathbf{r},\omega) &= -i\omega(\varepsilon(\mathbf{r},\omega)-\varepsilon_0)\tilde{\mathbf{E}}(\mathbf{r},\omega),\\ \tilde{\mathbf{P}}(\mathbf{r},\omega) &= (\varepsilon(\mathbf{r},\omega)-\varepsilon_0)\tilde{\mathbf{E}}(\mathbf{r},\omega).\end{aligned}$$

The total density is

$$\rho = -\nabla\cdot\mathbf{P}, \tag{8}$$

and the potential is obtained from the density by a convolution:

$$\phi(\mathbf{r},t) = \frac{1}{4\pi\varepsilon_0}\int\frac{\rho(\mathbf{r}',t)}{|\mathbf{r}-\mathbf{r}'|}d^3\mathbf{r}'. \tag{9}$$

(The numerical approach for calculating the convolution integral is discussed later.) The total field is made from any external fields applied as well as the contribution of the potential, i.e.,

$$\mathbf{E}(\mathbf{r},t) = -\nabla\phi(\mathbf{r},t) + \mathbf{E}_{ext}(t). \tag{10}$$

A proof that this description yields the correct frequency-dependent Poisson equation is straightforward and presented later. Note that Eqs. (3) and (9)–(10) also yield

$$\frac{\partial\mathbf{E}-\mathbf{E}_{ext}}{\partial t} + \frac{\mathbf{J}_T}{\varepsilon_0} = 0,$$

where

$$\mathbf{J}_T = \frac{1}{\nabla^2}\nabla\nabla\cdot\mathbf{J},$$

i.e., Eqs. (3) and (9)–(10) are equivalent to the Maxwell equation, except that the curl of the magnetic field is neglected.

Finally, note that the electric field is not propagated independently; only the currents and polarizations are integrated forward in time, as shown below.

B. Leapfrog propagation

Equations (5) and (6) are simplest to propagate forward in time in a leapfrog fashion; i.e., the currents $\mathbf{J}_j(\mathbf{r},t)$ are stored at times $dt/2, dt+dt/2, 2dt+dt/2, \ldots$, while the polarizations $\mathbf{P}_j(\mathbf{r},t)$ are stored at $0, dt, 2dt, \ldots$.

The discretization of the evolution equation for the current is then

$$\begin{aligned}&\frac{\mathbf{J}_j\left(\mathbf{r},t+\frac{1}{2}dt\right)-\mathbf{J}_j\left(\mathbf{r},t-\frac{1}{2}dt\right)}{dt}\\ &\quad= -\alpha_j(\mathbf{r})\frac{\mathbf{J}_j\left(\mathbf{r},t+\frac{dt}{2}\right)+\mathbf{J}_j\left(\mathbf{r},t-\frac{dt}{2}\right)}{2}\\ &\qquad-\bar{\omega}^2(\mathbf{r})\mathbf{P}_j(\mathbf{r},t)+\varepsilon_0\beta_j(\mathbf{r})\mathbf{E}(\mathbf{r},t),\end{aligned} \tag{11}$$

so that the evolution equation for the current is

$$\begin{aligned}\mathbf{J}_j\left(\mathbf{r},t+\frac{dt}{2}\right) &= \frac{1-\frac{\alpha_j(\mathbf{r})}{2}}{1+\frac{\alpha_j(\mathbf{r})}{2}}\mathbf{J}_j\left(\mathbf{r},t-\frac{dt}{2}\right)\\ &\quad-\frac{dt}{1+\frac{\alpha_j(\mathbf{r})}{2}}(\bar{\omega}^2(\mathbf{r})\mathbf{P}_j(\mathbf{r},t)-\varepsilon_0\beta_j(\mathbf{r})\mathbf{E}(\mathbf{r},t)).\end{aligned} \tag{12}$$

The evolution of the polarization is even simpler:

$$\mathbf{P}_j(t+dt) = \mathbf{P}_j(t) + dt\,\mathbf{J}_j\left(t+\frac{dt}{2}\right). \tag{13}$$

The initial conditions for the evolution are then

$$\mathbf{J}_j\left(t=-\frac{dt}{2}\right)=0,$$
$$\mathbf{P}_j\,(t=0)=0,$$
$$\mathbf{E}_{ext}(\mathbf{r}, t=m\,dt) = f(t=m\,dt)\mathbf{E}_0,$$

where $\mathbf{E}_0$ is the spatial profile of the external field (either uniform or concentrated in a given area); we chose a delta-function pulse for the time-dependent external field, i.e.,

$$f(t=m\,dt) = \begin{cases} 0, & m>0 \\ \dfrac{1}{dt}, & m=0 \end{cases},$$

but other choices, such as a step function, could have also been used.

In algorithmic form, the resulting formalism is straightforward:

Start with $\mathbf{J}_j = \mathbf{P}_j = 0$. Then, at each time step:

- First calculate the density, potential, and electric field.
- Then, update the current (Eq. (12));
- Finally, update the polarization (Eq. (13)).

The form of NF should allow for simple embedding, as discussed later.

C. Relation to frequency-space Poisson algorithm

The NF algorithm is reminiscent of two other formulations: Maxwell's FDTD, where the electric and magnetic fields are propagated rather than the polarizations, and where the current is also included; and the discrete dipole approximation.

The NF algorithm is also the time dependent version of the frequency dependent Poisson algorithm, whereby one solves

$$\nabla\cdot(\varepsilon(\mathbf{r},\omega)\nabla\tilde{\phi}) = -\nabla\cdot(\varepsilon(\mathbf{r},\omega)\tilde{\mathbf{E}}_{ext}(\mathbf{r},\omega)),$$

(i.e., the same as Eq. (4), with $\mathbf{E}=\mathbf{E}_{ext}-\nabla\phi$, and $\mathbf{E}_{ext}$ is the external field). The proof relies on the fact that the density and potential are related, from the potential's definition, by the usual Coulomb potential, so that, in frequency space,

$$\begin{aligned}
&\nabla\cdot(\varepsilon(\mathbf{r},\omega)\tilde{\mathbf{E}}(\mathbf{r},\omega)) \\
&= \nabla\cdot((\varepsilon(\mathbf{r},\omega)-\varepsilon_0)\tilde{\mathbf{E}}(\mathbf{r},\omega)) \\
&\quad +\varepsilon_0\nabla\cdot(\tilde{\mathbf{E}}(\mathbf{r},\omega)-\tilde{\mathbf{E}}_{ext}) + \varepsilon_0\nabla\cdot(\tilde{\mathbf{E}}_{ext}) \\
&= \nabla\cdot(\tilde{\mathbf{P}}(\mathbf{r},\omega)) - \varepsilon_0\nabla^2\tilde{\phi}(\mathbf{r},\omega) + \varepsilon_0\nabla\cdot(\tilde{\mathbf{E}}_{ext}) \\
&= -\tilde{\rho}(\mathbf{r},\omega) + \tilde{\rho}(\mathbf{r},\omega) + \varepsilon_0\nabla\cdot(\tilde{\mathbf{E}}_{ext}),
\end{aligned}$$

and if the external field is constant in space, the last term vanishes.

D. The convolution integral

A remaining issue is how to calculate the convolution integral. Here, we adopt the simplest approach, i.e., using a spatial Fourier transform; specifically, we write

$$\rho(\mathbf{r}) \to \tilde{\rho}(\mathbf{k}),$$
$$\tilde{\phi}(\mathbf{k}) = \frac{4\pi}{k^2}\tilde{\rho}(\mathbf{k}),$$
$$\tilde{\phi}(\mathbf{k}) \to \phi(\mathbf{r}).$$

For consistency, we also could use a similar approach when calculating the divergence of the polarization field, although we found in practice that the results are quite similar when a few-point formula is used for the calculation of the divergence.

There are many possible variations on this theme; for example, wrap-around effects can be accounted for by modifying the $4\pi/k^2$ coefficients; or the Poisson equation ($-\nabla^2\phi = \rho/\varepsilon_0$) could be solved explicitly by iterations; these variants will be explored in future work.

E. Extinction cross section

The extinction cross section is calculated by the usual formulae from the polarization or current. Specifically, we use a homogenous external field profile $\mathbf{E}_0\delta(t)$, which has a uniform frequency distribution ($\mathbf{E}_{ext}(\mathbf{r},\omega)=\mathbf{E}_0 = const.$) and get

$$\begin{aligned}
C_{ext} &= \frac{4\pi\omega}{c|\mathbf{E}_0|^2}\mathrm{Im}\left(\int \mathbf{P}(\mathbf{r},\omega)d\mathbf{r}\right)\cdot\mathbf{E}_0 \\
&= \frac{4\pi}{c|\mathbf{E}_0|^2}\mathrm{Re}\left(\int \mathbf{J}(\mathbf{r},\omega)d\mathbf{r}\right)\cdot\mathbf{E}_0,
\end{aligned} \tag{14}$$

where the Fourier transform has a unit overall coefficient (i.e., $\mathbf{J}(\mathbf{r},\omega)=\int_{-\infty}^{\infty}\mathbf{J}(\mathbf{r},t)e^{-i\omega t}dt$). Therefore, we just need, as usual, to calculate the total spatial current, integrate it over time, and Fourier transform to frequency space.

As a reminder, the presence of the velocity of light in this quasistatic expression is due to the definition of the extinction coefficient as the ratio of the energy-dissipation rate and the incoming flux, as the latter is proportional to c.

III. FITTING THE PERMITTIVITY OF GOLD AND SILVER

The parameters in the fit, α_j, $\bar{\omega}_j$, β_j, have a clear physical meaning from Eq. (2), as well known from textbooks and previous work. For each local "oscillator" j, α_j is the damping, $\bar{\omega}_j$ is the restoring frequency of the oscillator, and β_j (taken here as either positive or negative) is the contribution to the overall permittivity.

Here, we fitted the permittivity of gold and silver, over a wide frequency range (for gold 0.6–6.7 eV, the range of data for Johnson and Christy[14]). As mentioned above, there are several fits in the literature over narrower ranges, as well as a four-Lorentzians fit over the same range we covered (see Ref. 13 and references therein); these fits, however, have a wider range of values of the parameters. Here, a very large time step is used (2.5 a.u.); with such large time-steps, the

damping constants α_j and oscillator frequencies cannot be too large, so, as mentioned, a refit is necessary.

The fit was done by standard methods. An objective is defined:

$$I\{\alpha_j, \bar{\omega}_j\} = Min_{\{\beta_j\}}\left(\frac{1}{\text{eV}}\int g(\omega)(\text{Re}(\varepsilon(\omega) - \varepsilon_{exp}(\omega))^2 + C\text{Im}(\varepsilon(\omega) - \varepsilon_{exp}(\omega))^2)d\omega + \frac{10^{-5}}{(\text{eV})^2}\sum_j \beta_j^2\right). \quad (15)$$

For each value of the set of parameters, $\{\alpha_j, \bar{\omega}_j\}$ the optimal coefficients $\{\beta_j\}$ are found analytically by differentiation of the two terms in the right-hand side of Eq. (15) since the objective is bilinear in the coefficients, β_j. The objective functional with the optimal coefficients was minimized with respect to the nonlinear parameters, $\{\alpha_j, \bar{\omega}_j\}$, by a steepest descent algorithm, with the damping and restoring frequencies allowed to vary only in a restricted range,

$$0.1\,\text{eV} < \alpha_j < 2\,\text{eV},$$
$$0.001\,\text{eV} < \bar{\omega}_j < 1\,2\text{eV},$$

and we chose a weight function which will de-emphasize the lower frequency part where the permittivity is larger but has less structure: $g(\omega) = \frac{\omega^2}{\omega^2 + (1\text{eV})^2}$.

Note that since the coefficients $\{\beta_j\}$ are real we could treat the real and imaginary part in the objective independently; therefore, for the best fit we have set the coefficient of the imaginary part as $C = 10$.

Tables I and II show the fit parameters. Figures 1 and 2 show the quality of the fit over the Johnson and Christy range. As shown the fit is very accurate. Of course, in many simulations a lower quality fit (or the one tailored to a smaller specific region of frequencies) will suffice, so fewer terms could be used. A similar fit could have been applied to other metals; dielectrics would be more challenging, as mentioned.

Since the goal of the fit was numerical, we should be careful with allocating specific features in the permittivity (with their origin in inter- or intra- band transitions) to specific terms in the fit. However, we could tentatively relate some of the features of the permittivity to specific terms, for example, the features around 3 and 4 eV for gold or 4–5 eV for silver, where the permittivity changes rapidly.

TABLE I. Fitting parameters for gold.

$\bar{\omega}_j$ (eV)	α_j (eV)	β_j (eV)^2
0.2350	0.1551	95.62
0.4411	0.1480	− 12.55
0.7603	1.946	− 40.89
1.161	1.396	17.22
2.946	1.183	15.76
4.161	1.964	36.63
5.747	1.958	22.55
7.912	1.361	81.04

TABLE II. Fitting parameters for silver.

$\bar{\omega}_j$ (eV)	α_j (eV)	β_j (eV)^2
0.1696	0.1795	135.0
0.3655	0.2502	− 40.30
0.6312	2.114	− 50.06
1.175	1.627	16.73
2.077	1.820	7.651
4.018	1.049	− 15.36
4.243	0.9967	18.07
5.303	2.592	40.42
7.197	2.774	31.02

IV. RESULTS

To test NF we studied two types of systems: first, a single uniform gold or silver sphere; then, two uniform gold and silver spheres (more precisely balls) of 10 nm diameter as a function of the distance between them.

Most dimer simulations below included a grid of 64 × 32 × 32 points, with the grid spacing about 1/10th of the sphere radius; for single spheres, where high accuracy was required (as the results were compared to the analytical Mie theory, see below), we increased the number of grid points to $(64)^3$ and interpolated the results to the infinite-cell limit. Future publications will investigate the overall dependence on cell length.

We first study the extinction cross section for a single sphere. We scaled the results by the sphere volume and present below the scaled extinction cross section,

$$C'_{ext} \equiv \frac{C_{ext}}{V} = \frac{C_{ext}}{\frac{\pi d^3}{6}},$$

where d is the sphere diameter.

Figure 3 compares NF to the analytical solution of Maxwell's equations for a single sphere (Mie theory) for different sphere sizes. NF is formally exact in the long-wavelength limit, where the well-known extinction cross section is, from Mie theory,

$$C'_{ext} = \frac{C_{abs} + C_{scat}}{V} \cong \frac{C_{abs}}{V} = \frac{3\omega}{c}\text{Im}\left(\frac{\varepsilon - 1}{\varepsilon + 2}\right) \quad (\text{as } d \to 0), \quad (16)$$

and we introduce the absorption and scattering cross section, where the latter is negligible for small spheres.

As Fig. 3 shows, the numerical NF simulations agree with the exact Mie-theory Maxwell results for small spheres. For small diameters ($d = 1$ nm, $d = 10$ nm), the Mie-theory results equal to the limiting form in Eq. (16). The numerical NF simulations are slightly different from Eq. (16) due to grid-discretization and finite grid volume.

At low frequencies, where the wavelength is large, the larger-spheres Mie-theory results are reasonably similar to NF up to diameters of $d \sim 50$ nm; at higher frequencies, good agreement is obtained till $d \sim 30$ nm.

Figure 4 shows the evolution of the spectral shape for Maxwell's FDTD vs. NF as a function of spacing for both

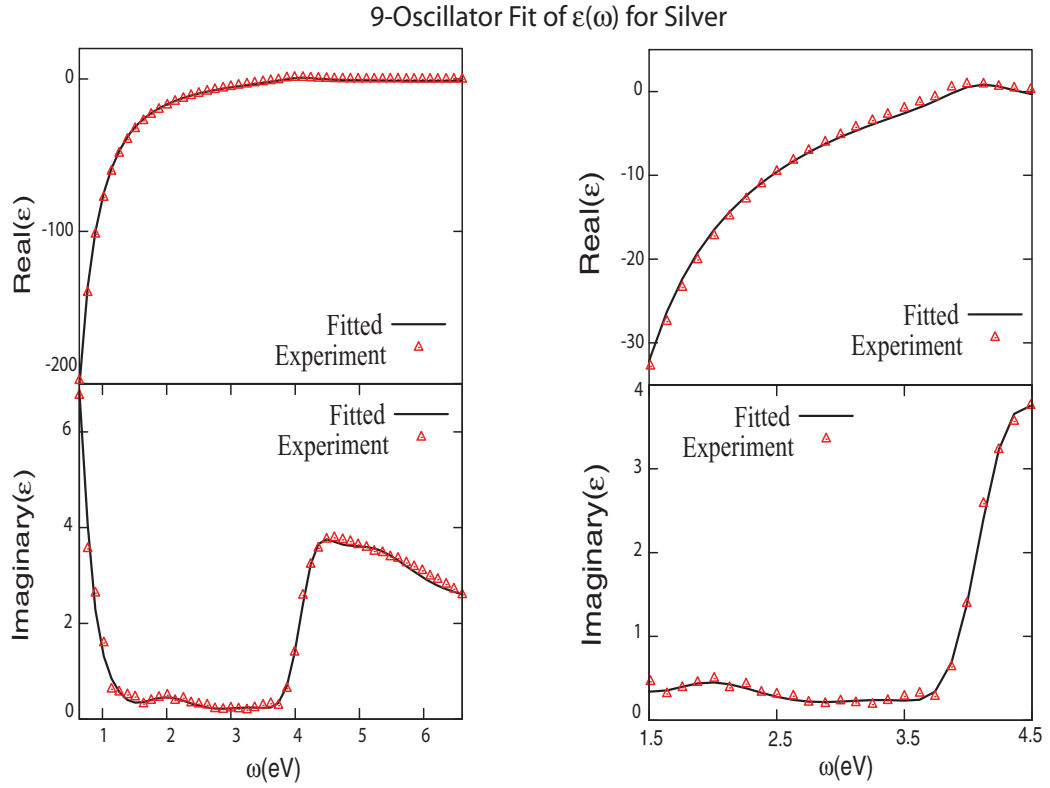

FIG. 1. Comparison of the fitted permittivity of silver: The Johnson-Christy data (triangles) vs. the new fit. The upper and lower panels show the real and imaginary parts. The left side shows the fit over a large range, and the right side zooms to a smaller frequency range, 1.5–4.5 eV.

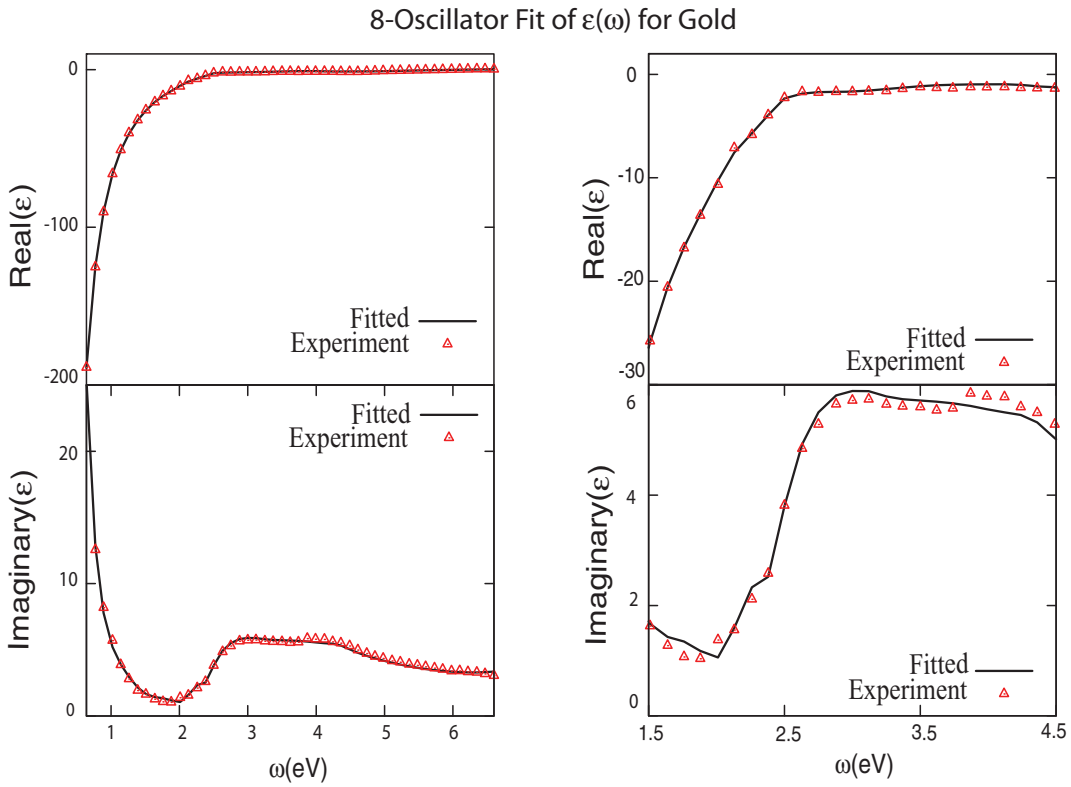

FIG. 2. Similar to Fig. 1, for gold, using 8 Lorentzians.

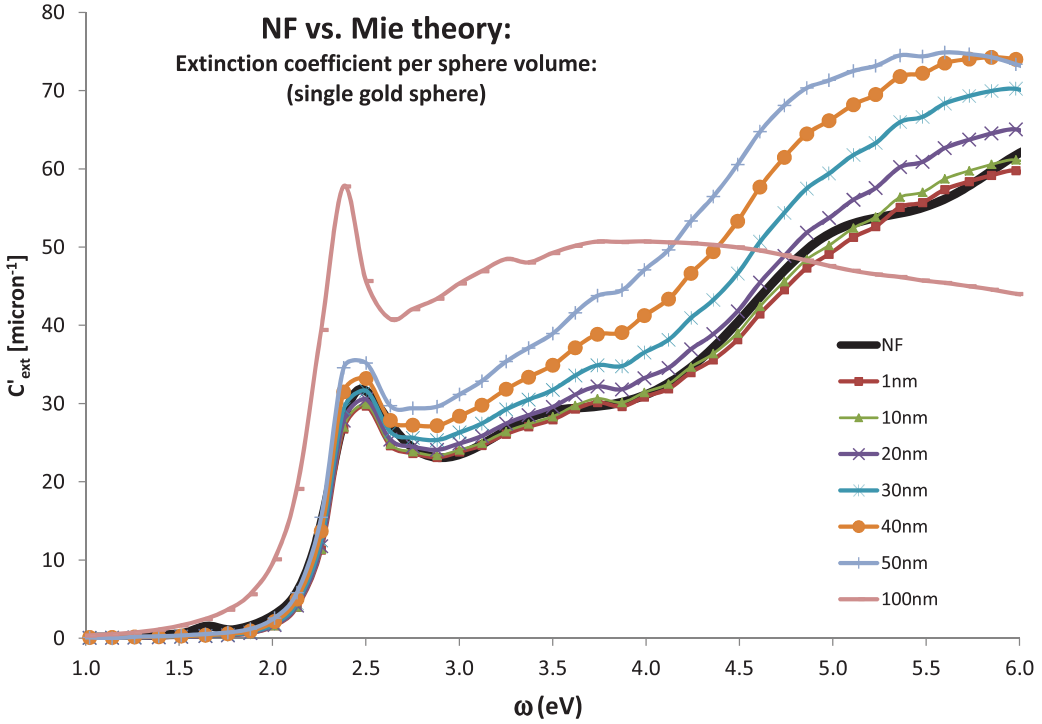

FIG. 3. Scaled extinction coefficient ($C'_{ext} \equiv C_{ext}/V$) for small gold spheres using both Mie theory at various sizes as well as NF. The Mie theory results are calculated and marked at the Johnson and Christy's experimental frequency point values.

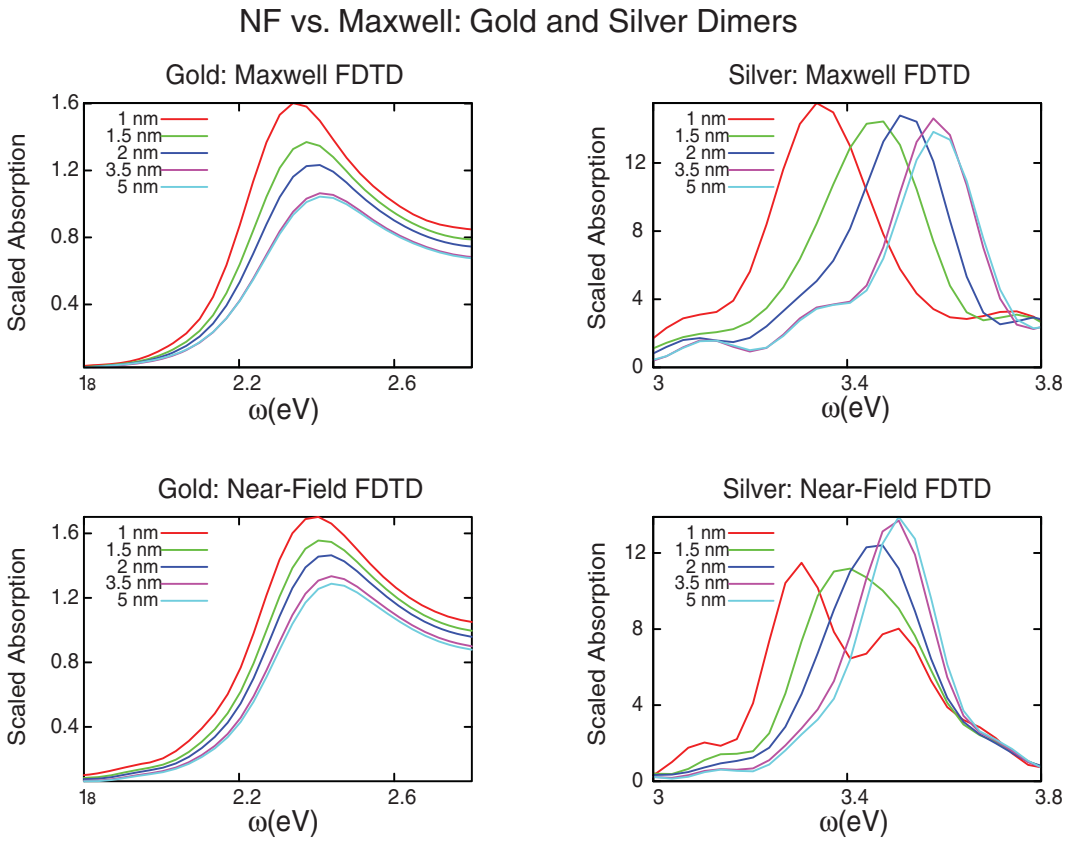

FIG. 4. Evolution of the spectral shape of the Maxwell FDTD (top) vs. NF(bottom) for spheres of diameter 10 nm, and an electric field parallel to the spheres. The left panels are for gold, and the right for silver. Each line refers to a different separation between the two spheres. Maxwell FDTD and NF agree well, and, in particular, NF shows the redshift that is expected with the decrease in the separation between the spheres.

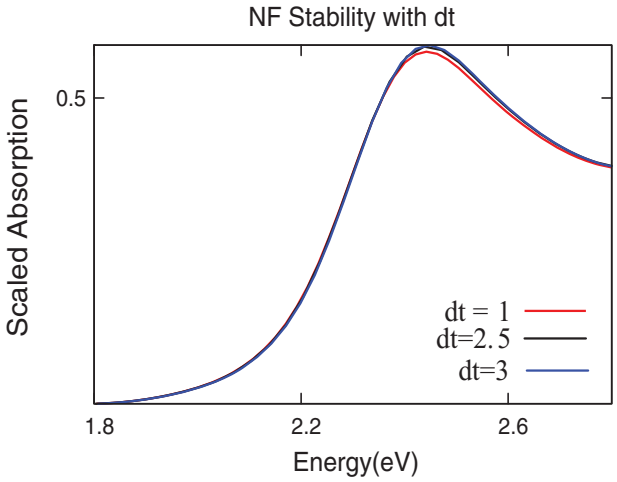

FIG. 5. NF is stable and accurate even for large time-step, as shown by the dependence of the absorption of a single gold sphere on time step. The figure shows that even for a time step of 3.0 a.u., the algorithm is convergent.

gold and silver dimers. The external electric field polarization is parallel to the dimer axis, and we study the absorption for different dimer spacings. The agreement is quite good. The lowering of the absorption peak at low separations[15] (essentially due to hybridization of the plasmon modes[16]) is evident, and reproduced very similarly in both approaches. There are some differences for small inter-sphere spacings; these are mostly due to the different spatial discretization schemes. NF uses a spatial-Fourier transform to calculate the electric field potential, rather than the nearest-neighbor spatial differences in Maxwell's FDTD.

Figure 5 shows that the method is well converged even for large time-steps.

Finally, Fig. 6 compares the electric field intensities for a challenging case, two silver spheres with a minimum distance of about 1 nm. The time-dependent electric fields were Fourier transformed at a frequency of 3.26 eV, and we show the intensity of the Fourier transformed fields along a slice in the x-y plane (near $z = 0$). The fields are quite similar; the differences are slightly due to the neglect of retardation effects in NF, but mostly due to the use of a different spatial discretization scheme. The intensities, which should be compared to the initial field intensity set at $|\tilde{E}_0(\boldsymbol{r}, \omega)|^2 = 1$ are quite large, due to the well-known enhancement of fields in confined regions near metal edges.

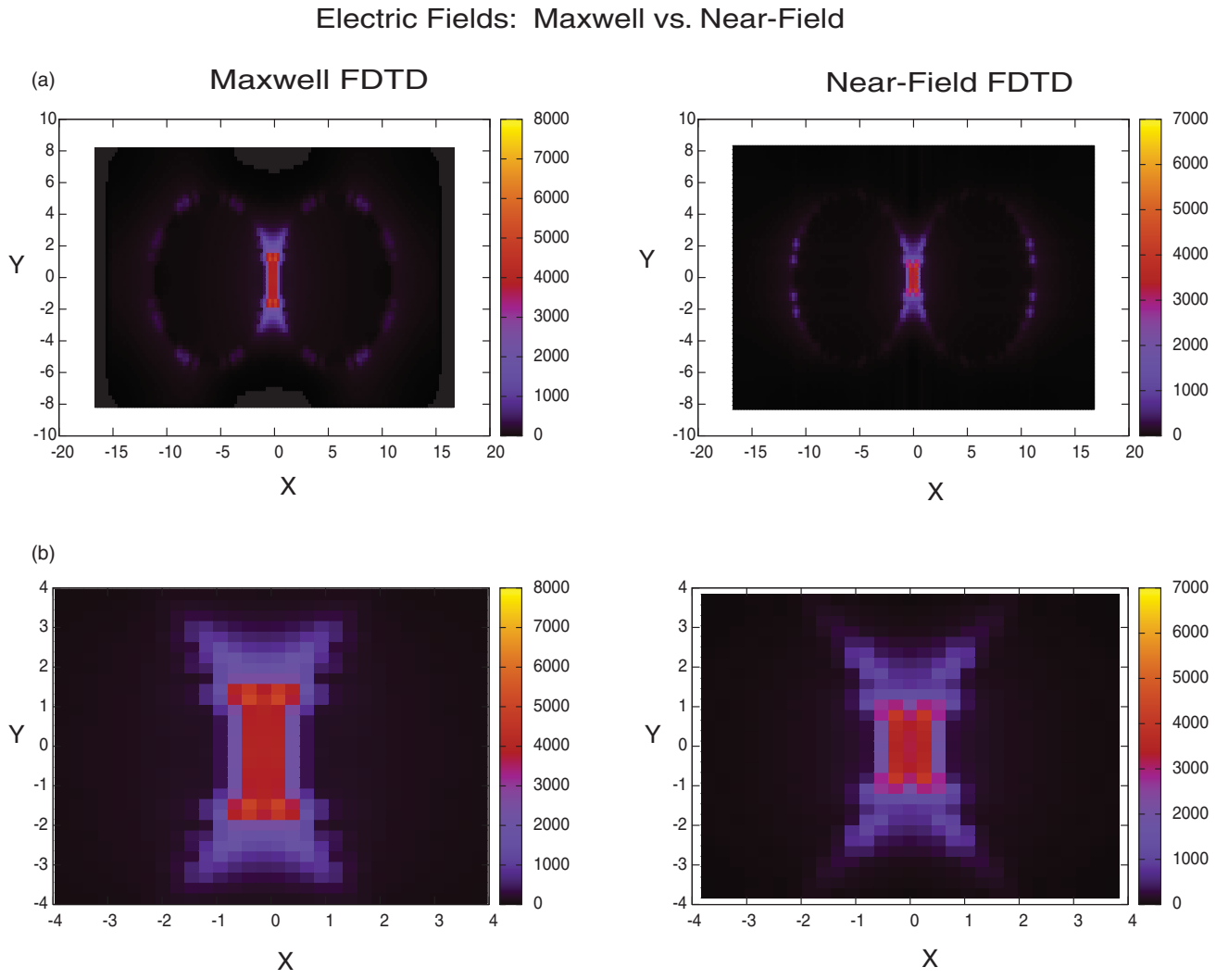

FIG. 6. A 2D cut, near $z = 0$, of the intensity of the electric fields at $\omega = 3.26$ eV in Maxwell-FDTD and NF. All x-y distances are in nm. The top panels encompass the full dimers, while the bottom panels zoom in to the central region and show clearly the high intensity between the spheres. For comparison, the intensity of the external electric field is normalized to 1.

V. DISCUSSION AND CONCLUSION

To summarize: The NF algorithm presented here is very efficient for systems with small scale dynamics, and enables very large time steps. There are several further improvements and extensions which are discussed in detail below.

A. Convolutions and dielectrics

There are two challenges in the approach as it stands. First is the use of a convolution to get the electric field from the density; this is quasilinear in the number of points (if an FFT convolution algorithm is used), so it will not slow the approach significantly, but an alternative approach to convolution will still be welcomed, as discussed below.

A different issue is, as mentioned, dielectrics, where the permittivity is almost constant over a large frequency range (and typically almost purely real). The difficulty is that the NF approach presented here requires that the frequency-independent term (associated with the first term in Eq. (2)) will be uniform (i.e., so that if a vacuum is used it equals ε_0), so that the Poisson equation could be easily solved. Possible solutions are as follows.

First is the combination of several terms as in Eq. (2) so that the sum of these terms will be fairly constant over a large frequency range; the difficulty is that then very wide Lorentzians (with large damping constants and large coefficients) will be needed, making the necessary time step quite small.

A second choice will be to use $\varepsilon_\infty = const.$, i.e., the same static term for all the materials. This choice would have been useful for the description of, e.g., metals with a single dielectric (e.g., water) without vacuum, where the same ε_∞ constant of the dielectric could be used for ε_∞ of the metal (at the cost of an additional fit of the metal parameters with the new ε_∞).

A more elegant solution allows for dielectrics with multiple different values of ε_∞ and has no convolutions. In this modification, the potential will be treated as an independent Car-Parinello type variable, and its evolution will be determined by

$$\mu\ddot{\phi} = -\left(\nabla\cdot(\varepsilon_s\nabla\phi) - \frac{\rho}{\varepsilon_0}\right), \tag{17}$$

where ε_s is the frequency-independent part of the permittivity instead of the first term (ε_0) of the RHS of Eq. (2) for metals. Here, μ is an artificial Car-Parinello type mass. Since this equation is scalar it could be solved with a smaller time step than that used in the main set of equations of the NF approach (Eqs. (5) and (6)) without loss of efficiency.

B. Embedding and magnetic fields

We note that the NF approach as presented here is ideal for embedding into it a smaller region where the material is presented more accurately. This will amount to adding an additional "quantum" current into the system, $\mathbf{J}_Q$, which will be propagated by more accurate approaches; either orbital-free TDDFT (time-dependent density functional theory), where the current is obtained by propagating a Schrödinger equation for a single orbital, or even TDDFT. The added current will be supplemented by an additional quantum density ρ_Q; embedding could be done by overlapping the two regions or by using a small transition region which will interpolate between the quantum and NF Poisson regions.

We also note that the method could potentially also be applicable to magnetic fields. While by its nature it cannot describe propagating far-field waves, it will be suitable to describe static magnetic fields or more generally near-fields due to the underlying currents. Details will be furnished in future publications.

C. Relation to FDTD features: Total-field scattered field (TF/SF) and absorbing layers

Finally, we comment on the equivalence in NF of two time-saving features in the usual Maxwell-FDTD.[3] The first is the TF/SF approach, where only the electric field in the inner scattered region is represented. This feature is automatically included in NF for most cases; for example, a planar incident field is represented by a spatially homogenous $\mathbf{E}_0$; the reason is that the k-dependence ($\exp(i\mathbf{k}\cdot\mathbf{r})$) of the incident field is ignored in NF, as it only deals with sub-wavelength features.

The second modern feature in FDTD is boundaries. Modern FDTD methods often employ the perfectly matched layers approach, which is essentially equivalent to exterior scaling in molecular scattering. NF could, in principle, have employed a similar approach; however, in practice, reflection is less of an issue in NF since the electric fields fall off quite rapidly in the subwavelength (near-field) regime. One could also pad the grids by a gradually rising layer of a conducting material, which will absorb any electric field which impinges on the boundaries. Detailed studies of the preferred approaches to handle boundaries will be presented in future publications.

ACKNOWLEDGMENTS

We are thankful for support by the National Science Foundation (NSF), Grant No. CHE-0810003.

[1] A. Taflove, Wave Motion **10**(6), 547 (1988).
[2] K. L. Shlager and J. B. Schneider, IEEE Trans. Antennas Propag. **37**(4), 39 (1995).
[3] A. Taflove and S. Hagness, *Computational Electrodynamics : The Finite-Difference Time-Domain Method*, 2nd ed. (Artech House, Boston, MA, 2000).
[4] C. Girard, Rep. Prog. Phys. **68**(8), 1883 (2005).
[5] S. K. Gray and T. Kupka, Phys. Rev. B **68**(4), 045415 (2003).
[6] B. T. Draine and P. J. Flatau, J. Opt. Soc. Am. A **11**(4), 1491 (1994).
[7] M. A. Yurkin and A. G. Hoekstra, J. Quant. Spectrosc. Radiat. Transf. **106**(1–3), 558 (2007).
[8] T. Jensen, L. Kelly, A. Lazarides, and G. C. Schatz, J. Cluster Sci. **10**(2), 295 (1999).
[9] P. Nordlander and E. Prodan, Nano Lett. **4**(11), 2209 (2004).
[10] D. J. Masiello and G. C. Schatz, J. Chem. Phys. **132**(6), 064102 (2010).
[11] Y. Sivan, S. Xiao, U. K. Chettiar, A. V. Kildishev, and V. M. Shalaev, Opt. Express **17**(26), 24060 (2009).
[12] K. Lopata and D. Neuhauser, J. Chem. Phys. **131**(1), 014701 (2009).
[13] F. Hao and P. Nordlander, Chem. Phys. Lett. **446**(1-3), 115 (2007).
[14] P. B. Johnson and R. W. Christy, Phys. Rev. B **6**(12), 4370 (1972).
[15] S. A. Maier, P. G. Kik, and H. A. Atwater, Appl. Phys. Lett. **81**(9), 1714 (2002).
[16] P. Nordlander, C. Oubre, E. Prodan, K. Li, and M. I. Stockman, Nano Lett. **4**(5), 899 (2004).